



Aerodynamic performance assessment of ϕ -type vertical axis wind turbine under pitch motion



Jie Su^a, Yu Li^a, Yaoran Chen^a, Zhaolong Han^{a, b, c, d, *}, Dai Zhou^{a, b, c, d, **}, Yongsheng Zhao^{a, b}, Yan Bao^a

^a School of Naval Architecture, Ocean and Civil Engineering, Shanghai Jiao Tong University, Shanghai, 200240, People's Republic of China

^b State Key Laboratory of Ocean Engineering, Shanghai Jiao Tong University, Shanghai, 200240, People's Republic of China

^c Key Laboratory of Hydrodynamics of Ministry of Education, Shanghai Jiao Tong University, Shanghai, 200240, People's Republic of China

^d Shanghai Key Laboratory for Digital Maintenance of Buildings and Infrastructure, Shanghai Jiao Tong University, Shanghai, 200240, People's Republic of China

ARTICLE INFO

Article history:

Received 19 July 2020

Received in revised form

8 February 2021

Accepted 21 February 2021

Available online 26 February 2021

Keywords:

Aerodynamic performance

ϕ -type vertical axis wind turbine

Pitch motion

IDDES

ABSTRACT

The floating vertical axis wind turbine (VAWT) is considered as a competitive device in the utilization of offshore wind energy. However, the platform pitch motion would affect its aerodynamic behavior. In this paper, the aerodynamic performance of a floating ϕ -type VAWT under pitch motion is investigated by using the Improved Delayed Detached Eddy Simulation SST $k - \omega$ turbulence model. After verifying the feasibility of the numerical model, the effects of pitch motion amplitude and period on the aerodynamic characteristics were evaluated, and the impacts of these observations were elucidated. The results showed that the averaged net power coefficient increment of about 1.5%–15% could be obtained under platform pitch motions, and the fluctuation of aerodynamic loads was found to increase. Besides, the pitch motion pattern could be regarded as the combination of surge and heave motions, which explained the similarity of their effects on the wind turbine aerodynamics. Furthermore, it was found that the frequency of the peak torque coefficient would change under different periods of pitch motion, which should be noticed in the design of floating wind turbine. Finally, it was concluded that the current study provided additional information about the effect of pitch motion on wind turbine aerodynamics.

© 2021 Elsevier Ltd. All rights reserved.

1. Introduction

In recent years, with the continuous changes in the international situation, the development of marine resources has become the focus of strategic development of countries in the world. There are a great amount of wind energy resources in the offshore and deep-sea areas. Compared with fossil fuel power generation, the advantages of wind power generation in the economic field gradually become obvious [1,2]. In view of that it is increasingly difficult to find areas with good wind energy potential on land [3], the need to

further exploit the offshore wind energy resources is highlighted. In this context, the offshore floating wind turbines have attracted more public attention.

The wind turbine can be mainly divided into two categories: horizontal axis wind turbines (HAWTs) and vertical axis wind turbines (VAWTs). Due to the great amount of efforts made on the HAWT, this kind of wind turbine has become the most acceptable wind conversion device with the largest market in the world. On the contrary, the lower power coefficient has hindered the application of the VAWT. The small-scale VAWTs are usually installed in the urban area [4], which has more complex wind flow conditions. However, facing the trend of offshore wind resources utilization, the VAWT has shown some advantages over the HAWT. It is known that the gear box, generators, yaw device and other engine room power equipment are installed in the nacelle on the top of the HAWT tower. These heavy equipment installed in high places are detrimental to the structural safety of the wind turbine tower, and the installation and maintenance costs are quite high, especially in the context of floating wind turbine applications. Compared with

* Corresponding author. School of Naval Architecture, Ocean and Civil Engineering, Shanghai Jiao Tong University, Shanghai, 200240, People's Republic of China.

** Corresponding author. School of Naval Architecture, Ocean and Civil Engineering, Shanghai Jiao Tong University, Shanghai, 200240, People's Republic of China.

E-mail addresses: han.arkey@sjtu.edu.cn (Z. Han), zhoudai@sjtu.edu.cn (D. Zhou).

that, the generators and nacelle of VAWT are usually installed in the bottom of the wind turbine tower. This approach, as well as other benefits including lower maintenance cost, no yaw device and suitability for turbulent wind flow [5], has made the VAWT sufficiently competitive in the offshore wind utilization and brought new impetus to its development.

It is generally considered that the bottom-mounted wind turbines, including those with monopile foundation, tripod support, or jacket structure [6,7], are more preferable in the offshore region. But for the deeper waters (> 50 m water depth), the floating wind turbine presents superiority in supporting structure and economics compared with the former one [8]. Therefore, in the last decade, a series of studies has been conducted on the feasibility of floating wind turbine, especially for the HAWTs [9–12]. The scope of the research mainly includes the platform motion patterns [9], aerodynamic performance [10], structural response [11,12], damping effect [13], and active control [14].

Among these problems, the coupling effect of aerodynamic force on the platform motion is one of the most important issues that has been studied in depth. Since the Froude and Reynolds scaling rules cannot be satisfied simultaneously in the wind/wave basin test, the floating wind turbine model is usually dominated by the Froude scaling rule with the correction of aerodynamic loads [9]. To ensure the similarity of wind turbines' power and thrust and evaluate the influence of aerodynamic force, many methods have been developed, including the redesigned shape of rotor blades, different blade surface roughness, and controlled ducted fan [15]. After basically solving the aerodynamic simulation problem, the motion response of the floating wind turbine was analyzed under different environmental conditions [16,17]. Besides, Koo et al. [18] experimentally studied the motion response of a floating wind turbine on three different floaters. It was found that the wind load would increase the surge and pitch damping of the spar-buoy and semi-submersible. Karikomi et al. [13] investigated the negative damped response of floating wind turbines by wind tunnel testing. The effect of bandwidth of the rotor speed controller on the platform stability was studied to suppress the negative damped response. Furthermore, for the active wind turbine control scheme, Goupee et al. [14] evaluated the effect of blade pitch and generator controls on the global response of a floating HAWT. The results showed that the variable speed control scheme effectively reduced the platform pitch motions compared with that of the constant rotor speed control. These active turbine controls were thought to be beneficial to the floating wind turbine. Similarly, Madsen et al. [19] applied different control strategies, including two closed-loop controllers and one open-loop controller, to the floating wind turbine. It was reported that the conventional onshore controller might cause high oscillations in blade pitch.

For the offshore floating VAWT, the progress of relevant research work is relatively slow, while it was reported to achieve about 20% reduction in cost of energy compared with that of HAWT by Paquette and Barone [20]. Most of the existing research is focused on the dynamic response of floating VAWT. Similar to the research method of floating HAWT mentioned above, the VAWT model has also been tested on different floating support structures by Borg and Collu [21]. It was reported that the traditional spar and tension-lag-platform could not sufficiently restrain the motion of floating VAWT due to its complex aerodynamic load. Afterwards, the stochastic dynamic response and wind-wave coupling effect of a floating VAWT with the semi-submersible platform were analyzed by Wang et al. [22] and Cheng et al. [23]. Recently, the coupling motion of a ϕ -type VAWT with a redesigned truss spar was investigated [24]. It was found that the regular wave frequency dominated the frequencies of platform surge, heave and pitch motions.

Although there are numerous studies conducted on the dynamic response of floating wind turbine, the effect of platform motion on its aerodynamic characteristics was seldom investigated, especially for the floating VAWT. In the previous studies, the methodology utilized to simulate the aerodynamic force mainly includes the blade element moment theory [25] and Cascade model [26]. In recent years, a few studies investigating the aerodynamics of a floating H-type VAWT by computational fluid dynamics (CFD) have been reported [27,28]. For instance, Lei et al. [28] verified the applicability of the Detached Eddy Simulation to the aerodynamic performance of floating H-type VAWTs. The study found that platform motion would enhance the interaction between the flow field and wind turbine blades.

The ϕ -type VAWT is regarded as another typical wind turbine configuration, which has advantages in terms of structural load [29]. Due to its distinctive shape, the aerodynamic performance is different from that of H-type wind turbine reported in previous work [28]. However, the aerodynamics of the ϕ -type VAWT under platform motion has rarely been investigated, and its increased fluctuation of aerodynamic forces also requires further investigation. Furthermore, more attention should be paid to the change in the frequency of aerodynamic load history caused by the platform motion.

In the current study, the aerodynamic performance of a ϕ -type Darrieus VAWT under pitch motion was studied. A typical small-scale ϕ -type VAWT model was selected to investigate its aerodynamic characteristics under fixed and moving conditions. In practical offshore wind farm project, the size of wind turbine is usually over 100 m. Thus, the scale ratio was set as 1:20 in this study, and all results could be processed to reflect the real responses of large-scale wind turbines according to the Froude and Reynolds similarity criteria. In this study, a series of high-fidelity CFD simulations were carried out using the Improved Delayed Detached Eddy Simulation (IDDES) SST $k - \omega$ turbulence model. The geometric model and operational characteristics of the VAWT were presented, and the computational model as well as numerical settings was described in Section 2. The model validations, including time step independence test, mesh scheme analysis, and model verification, were conducted in Section 3. After that, Section 4 presented the comparison of aerodynamic performance of VAWT under different conditions. Meanwhile, the effect of amplitude and period of pitch motion was discussed. Besides, the results of the studied ϕ -type VAWT were compared with the H-type wind turbine. In addition, the result analysis in the frequency domain was carried out to gain insights into the aerodynamic behaviors. The reasons for the difference in the results of the two types of wind turbine, as well as the influence of peak frequency were also discussed. Afterwards, a discussion on the correlation between the pitch motion of wind turbine and the aerodynamics was conducted in Section 5. Finally, several main conclusions were summarized in Section 6.

2. Methodology

2.1. Geometric model

The prototype of the typical ϕ -type Darrieus VAWT tested by Sheldahl et al. [30] was selected in this study. The profile NACA0015 was utilized to design the rotor blade. The details of geometric parameters of the studied Darrieus VAWT are shown in Table 1, and the model of the ϕ -type wind turbine is illustrated in Fig. 1. To simplify the model, the shaft and struts are neglected in the current study. Besides, considering the difficulties in constructing Darrieus rotor with ideal Troposkein shape, the parabolic approximation was

Table 1
The geometric parameters of the φ -type Darrieus VAWT.

Property	Symbol	Value
Airfoil profile	–	NACA 0015
Chord length	c	0.1524 m
Angular speed	Ω	162.5 rpm
Equatorial diameter	D	5.00 m
Rotor height	H	5.10 m
Swept area	A	17.01 m ²
Rated power	–	2 kW

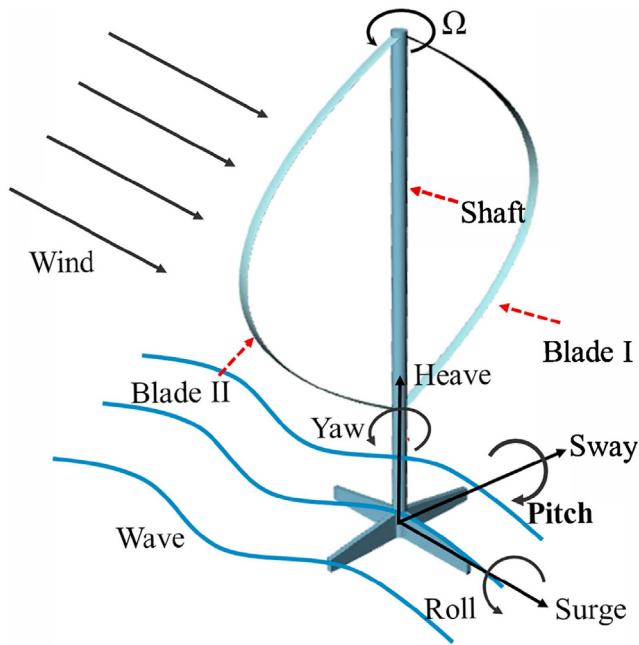


Fig. 1. The structure of the floating φ -type Darrieus VAWT.

used to describe the relationship between the local radius and altitude due to its superiorities in geometric similarity and modeling simplicity [31]. In this study, the relationship between local radius r and local altitude z is described by a parabolic equation, written as:

$$r = -\frac{R}{(H/2)^2} \left(z - \frac{H}{2} \right)^2 + R \quad (1)$$

where R is the equatorial radius and H is the rotor height. The range of local altitude z is $[0, H]$.

The power coefficient of the φ -type wind turbine can be written as:

$$C_p = \frac{Q_{torque} \Omega}{\frac{1}{2} \rho U_\infty^3 A} \quad (2)$$

where Q_{torque} , Ω , U_∞ , A and ρ are the generated torque, angular velocity, free-stream velocity, rotor swept area and air density, respectively.

Similarly, the torque coefficient C_Q , lateral force coefficient $C_{lateral}$, and thrust coefficient C_{thrust} can be calculated as:

$$C_Q = \frac{Q_{torque}}{\frac{1}{4} \rho U_\infty^2 A D} \quad (3)$$

$$C_{lateral} = \frac{F_{lateral}}{\frac{1}{2} \rho U_\infty^2 A} \quad (4)$$

$$C_{thrust} = \frac{F_{thrust}}{\frac{1}{2} \rho U_\infty^2 A} \quad (5)$$

where $F_{lateral}$ and F_{thrust} are the forces exerting on the rotor, and the directions are along cross-wind direction and stream-wise direction, respectively.

For the studied φ -type VAWT, the definition of azimuthal angle of 0° is shown in Fig. 2. The region from $\theta = 90^\circ$ to $\theta = 270^\circ$ can be defined as the upwind region, while the region $\theta = 270^\circ \sim 0^\circ \sim 90^\circ$ is the downwind region.

Besides, to simulate the pitch motion of the φ -type VAWT, the whole rotor was assigned the motion rules by using a user-defined function. A prescribed pitch motion with a harmonic displacement against time was introduced. The pitch motion can be represented as:

$$\beta_{pitch} = A_{amp} \cdot \sin(2\pi f t) \quad (6)$$

The angular velocity induced by the pitch motion can be written as:

$$\omega_{pitch} = 2\pi f A_{amp} \cdot \cos(2\pi f t) \quad (7)$$

where A_{amp} , f , and t are the angular amplitude, frequency of pitch motion, and time, respectively.

2.2. Computational model

As shown in Fig. 3, an elaborate three-dimensional computational domain was built to analyze the aerodynamic performance of the φ -type VAWT. To meet the requirements of blocking rate in the simulation and ensure the full development of wind turbine wake as recommended by Thé and Yu [32], the length, width, and height of the computational domain were set as $20D$, $10D$, and $4H$ [33], respectively. The wind turbine was located $5D$ downstream from the inlet boundary. Besides, the computational model was divided into two regions: the rotational region and the stationary region. The rotational region was elaborately designed to reduce the computational cost. The quadratic curve of the blade was utilized to create such a spindle-shaped region as illustrated in Fig. 3. The size of the cross section of this region was $10c \times 10c$.

Besides, to simulate the pitch motion of the wind turbine, the overset mesh technique was utilized. The surfaces between these two regions were set as interfaces, where the linear interpolation

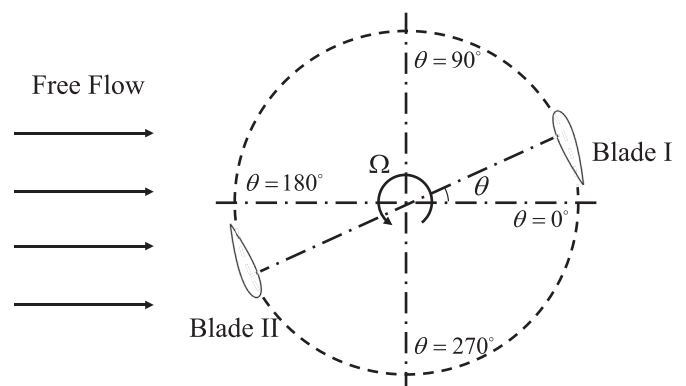


Fig. 2. The top view of the equatorial section of the wind turbine.

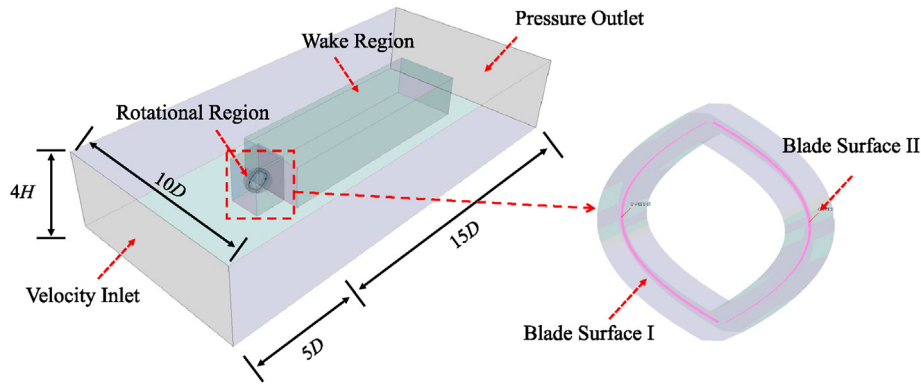


Fig. 3. The three-dimensional computational domain built in this study.

method was selected to exchange the data after each time step. For the boundary conditions, the surface of blade, the inlet and outlet boundary were set as no-slip wall condition, velocity inlet ($U_\infty = 8.5$ m/s), and pressure outlet (0.0 Pa), respectively. The turbulence intensity in this model was 0.01, and the turbulent viscosity ratio was set as 10. Besides, the other four sides of the model were assumed as slip walls.

2.3. Numerical settings

In the current study, the three-dimensional incompressible flow was simulated by the commercial software STAR-CCM+ (version 13.04). The implicit unsteady segregated flow method was selected to solve the discretized continuity and momentum equations. The IDDES SST $k - \omega$ turbulence model was adopted to solve the flow field due to its superiority in solving the flow field around the wind turbine [27,34]. The second-order difference formula was performed for the discretization. The SIMPLE scheme was used to solve the pressure-velocity coupling equation and the IDDES turbulence model. To make the residuals small enough, a maximum of 20 iterations were performed in each time step. To improve the computational efficiency, 40 parallel CPU cores were utilized to solve the model. All the simulations were performed on a small-scale Server with two Intel(R) Xeon(R) CPUs (E5-2630 v3), 128 GB memory, and 2T hard drive. It takes about 576 h to complete twelve revolutions calculation.

3. Model validation

3.1. Time step independence test

Different time steps will affect the calculation accuracy and computational efficiency. Thus, it makes sense to determine the appropriate time step size. Three different time step schemes ($\Delta t_1 = T/90, \Delta t_2 = T/180, \Delta t_3 = T/360$) were selected to evaluate their effects on the target function, torque coefficient C_Q , at tip speed ratio $\lambda = 5.0$.

The variations of torque coefficient are shown in Fig. 4. It can be found that with decreasing the time step size, the torque coefficient curves of Δt_2 and Δt_3 are almost overlapped while the curves of Δt_1 is different. For the calculation efficiency, therefore, the time step scheme $\Delta t_2 = T/180$ was select for the simulations.

3.2. Mesh independence analysis

To find out an efficient mesh scheme for the model, the mesh independence test was carried out. The mesh topology of the

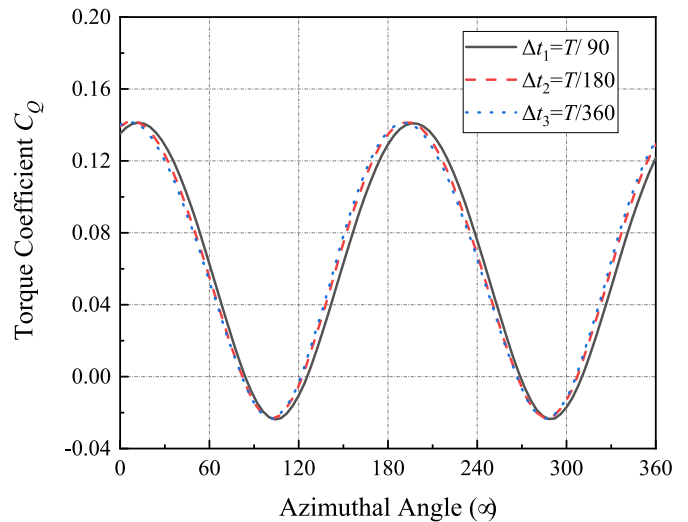


Fig. 4. Comparison of torque coefficient variations under three different time steps.

computational domain is illustrated in Fig. 5. The orthogonal prismatic meshes were created on the blade surfaces while the volume meshes were made by trimmed mesher. Three mesh schemes with different resolutions in the rotational region were analyzed at tip speed ratio $\lambda = 5.0$ as shown in Table 2. There are 154 grid points around the wind turbine blade in the medium mesh scheme, and the maximum surface growth rate was 1.2, which controls the grid point distribution. Besides, there are 20 layers of prismatic layer cells created on the blade surfaces, and the thickness of the first layer cell was 7×10^{-6} m with growth ratio of 1.25. In this way, the obtained wall function y^+ was approximately equal to 1. In this study, the Reynolds numbers are about $Re = 1.5 \times 10^5 \sim 5.0 \times 10^5$.

The comparison of power coefficients C_p obtained at $\lambda = 5.0$ under the three mesh schemes is presented in Table 2. The results indicate that the error of averaged power coefficient decreases when the meshes around the blade are refined. The difference in C_p between the medium mesh and fine mesh is less than 2.5%. Therefore, the medium mesh scheme was considered an acceptable mesh resolution, and it was used in the following simulations.

3.3. Validation test

To verify the capability of numerical model in simulating wind energy conversion efficiency of the studied ϕ -type VAWT, the validation test was conducted at different tip speed ratios, and the

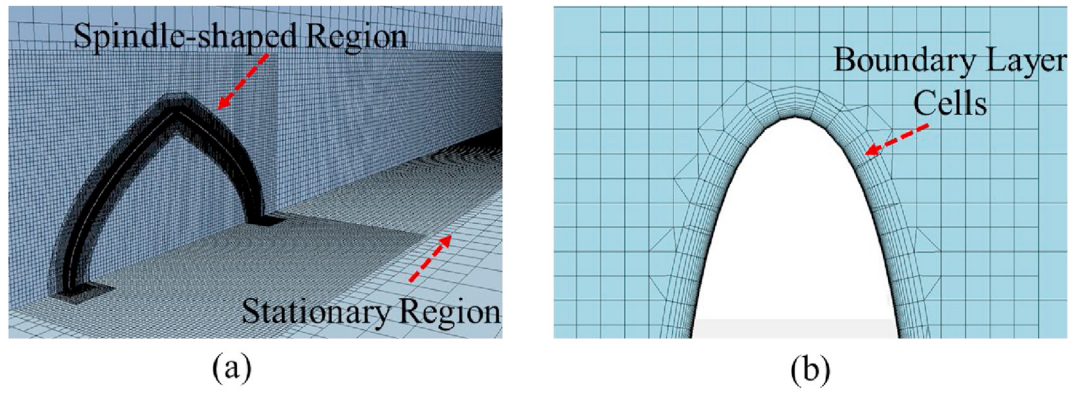


Fig. 5. The mesh topology of the computational domain: (a) refined mesh; (b) boundary layer cells.

Table 2
Comparison of power coefficient under different mesh schemes ($\lambda = 5.0$).

Mesh Scheme	Total number of grids	Power coefficient C_p	Relative error
Coarse	18.0 million	0.2974	8.63%
Medium	20.0 million	0.3177	2.40%
Fine	22.7 million	0.3255	–

results were compared against the experimental data [30]. The numerical settings are consistent with the experimental conditions, and all the other parameters used in the simulation are the same as mentioned in Section 2.3.

Fig. 6 illustrates the comparison of the current results and the experiments, where the power coefficient C_p was utilized to evaluate the errors. Here, the relative error is defined as the ratio of the absolute error between current results and the experiments to the experimental value. It can be found that the trend of power coefficient C_p of the present study is basically in line with the experimental data. The minimum relative error is 1.98% while the maximum relative error of 11.01% occurs at tip speed ratio $\lambda = 2.0$. The error may be partly due to the parabolic approximation of the wind turbine, and this approximation is generally accepted [31,35]. Besides, the simplification of the computational model, as well as the difference between simulation and field test, would also cause errors.

In addition, another numerical validation for the aerodynamics

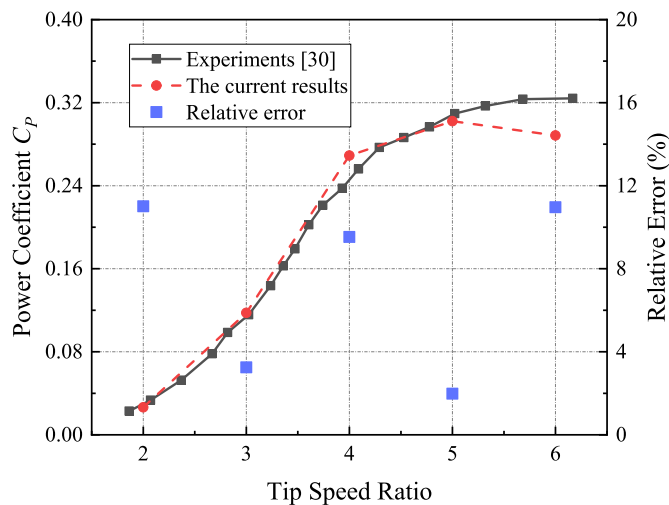


Fig. 6. Comparison of the current results and the experimental data [30].

of the wind turbine under pitch motion was conducted due to lack of experimental data on floating wind turbines. The three mesh schemes mentioned in Section 3.2 were also tested for moving wind turbine shown in Table 3. The results indicate that the relative error of averaged power coefficient of pitch VAWT decreases when the meshes are refined. Overall, the results indicate that the current numerical model could be considered an acceptable approach to investigate the aerodynamic performance of such ϕ -type VAWT for the rest simulations.

4. Results

The pitch motion of the ϕ -type VAWT follows equation (6) described in Section 2.1. In one period of pitch motion, the spatial position of wind turbine changes as shown in Fig. 7. The sequence of pitch motion is defined as 1 \rightarrow 2 \rightarrow 3.

According to the literature [36,37], the inclination angle of offshore platform should be controlled within 15°. Thus, the maximum pitch angle of 15° was selected while the period of pitch motion T_{pitch} was set to four times T (T is the rotor rotation period) in this subsection. The variations of pitch angle and angular velocity are shown in Fig. 8. To evaluate the effect of pitch motion on the aerodynamics of wind turbines, all the simulations were conducted at tip speed ratio $\lambda = 5.0$. Besides, it should be noticed that the azimuthal angle of blade I was set to $\theta = 0^\circ$ at $t = 0$ in one pitch period.

In addition, the results of the present study could be utilized to evaluate the performance and responses of large-scale wind turbine according to the Froude and Reynolds similarity criteria. It should be noted that the size of real life large-scale wind turbine is usually over 100 m in practical offshore wind farm project. Thus, the scale ratio was set as 1:20 in this study. The wind turbine was simulated under given platform motion. It was assumed that the platform motion patterns set in this study were caused by the real waves. According to the Froude and Reynolds similarity criteria, the rotor revolution period is 0.370s and the pitch motion period is 1.478 s at tip speed ratio of 5 for the small-scale model, while the rotor revolution period is 1.653s and the pitch period is 6.612s for

Table 3
Comparison of power coefficient of the pitching VAWT under different mesh schemes ($\lambda = 5.0, A_{amp} = \pi/12, T_{pitch} = 4T, T$ is the rotor rotation period).

Mesh scheme	C_p of pitching VAWT	Relative error
Coarse	0.3373	7.16%
Medium	0.3530	2.84%
Fine	0.3633	–

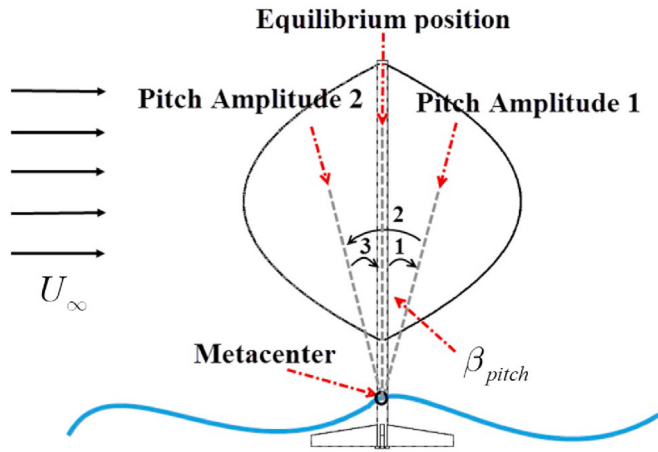


Fig. 7. The pitch motion pattern of the ϕ -type VAWT.

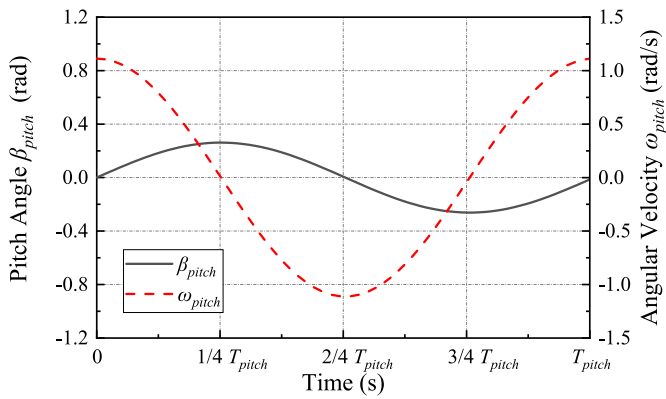


Fig. 8. The variation of pitch angle and angular velocity ($A_{amp} = \pi/12, T_{pitch} = 4T$).

the large-scale model. Besides, the effect of tip speed ratio on the wind turbine performance was also studied. It means that the range of rotor revolution period is 0.308s~0.924s and the pitch period is 1.232s~3.696s for the small-scale model, while the rotor revolution period is 1.377s~4.132s and the pitch period is 5.510s~16.529s for the large-scale wind turbine.

4.1. Aerodynamic performance

The variations of torque coefficient of the wind turbine versus time are illustrated in Fig. 9. It can be found that the fluctuation of torque coefficient C_Q of the ϕ -type wind turbine in pitch motion is much greater than that of the fixed VAWT. In the first stage of pitch motion ($t = 0 \sim 1/4T_{pitch}$), the torque coefficient of the moving VAWT is smaller than that of the fixed one. After that, the torque generated by the moving wind turbine dramatically increases, and the maximum C_Q occurs at $t = 2/4T_{pitch}$, where the VAWT returns to the equilibrium position. After $t = 2/4T_{pitch}$, the generated torque decreases. This fluctuation is due to the effects of the induced velocity caused by the pitch motion. During the time $[0, 1/4T_{pitch}]$ and $[3/4T_{pitch}, 4/4T_{pitch}]$, corresponding to the phases 1 and 3 of the pitch motion defined in Fig. 7, the direction of horizontal component of induced velocity is consistent with that of the free-stream wind. Thus, the incoming flow velocity decreases for the VAWT, resulting in the lower relative local velocity for the blade. On the contrary, the direction of horizontal component of induced velocity is opposite to that of wind during the time $[1/4T_{pitch}, 3/4T_{pitch}]$ (phase 2 of the pitch motion). Therefore, the relative local velocity increases and the torque output is larger.

Similarly, the trend of torque coefficient of one single blade can be found as shown in Fig. 9 (b). In this case, the period of pitch motion T_{pitch} was set to four times the rotor rotation period. Thus, four complete cycles of the torque coefficient variation can be seen. It is clear that the torque coefficient curves in each rotation cycle are basically the same for the fixed VAWT, while the coefficient curve of the moving wind turbine varies greatly in different rotation cycles. The peak value of torque coefficient occurs in the up-wind region (about $\theta = 182^\circ$), and the lowest torque occurs at about $\theta = 88^\circ$. The similar phenomena were also reported in the investigations of H-type VAWT conducted by Lei et al. [28]. It indicates that the energy extraction for the pitching VAWT is more unbalanced during rotor rotation compared with the stationary wind turbine. It would also increase the fatigue load of the blades and exacerbate the durability problems of the wind turbine.

To make further investigation on the aerodynamic behavior, the static pressure coefficient on the blade surface were calculated. Due to the characteristics of pitch motion, the induced velocities are different at different altitudes. Thus, the pressure coefficient distributions on different sections along the blade span at different

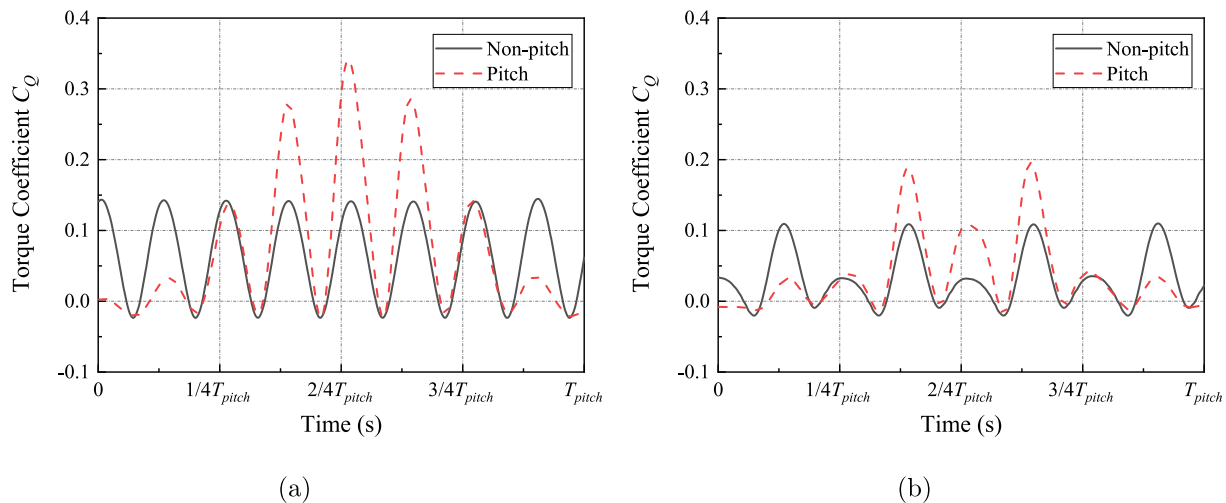


Fig. 9. The variations of torque coefficient in one period of pitch motion: (a) the whole rotor; (b) blade 1 ($\lambda = 5, A_{amp} = \pi/12, T_{pitch} = 4T, T$ is the rotor rotation period).

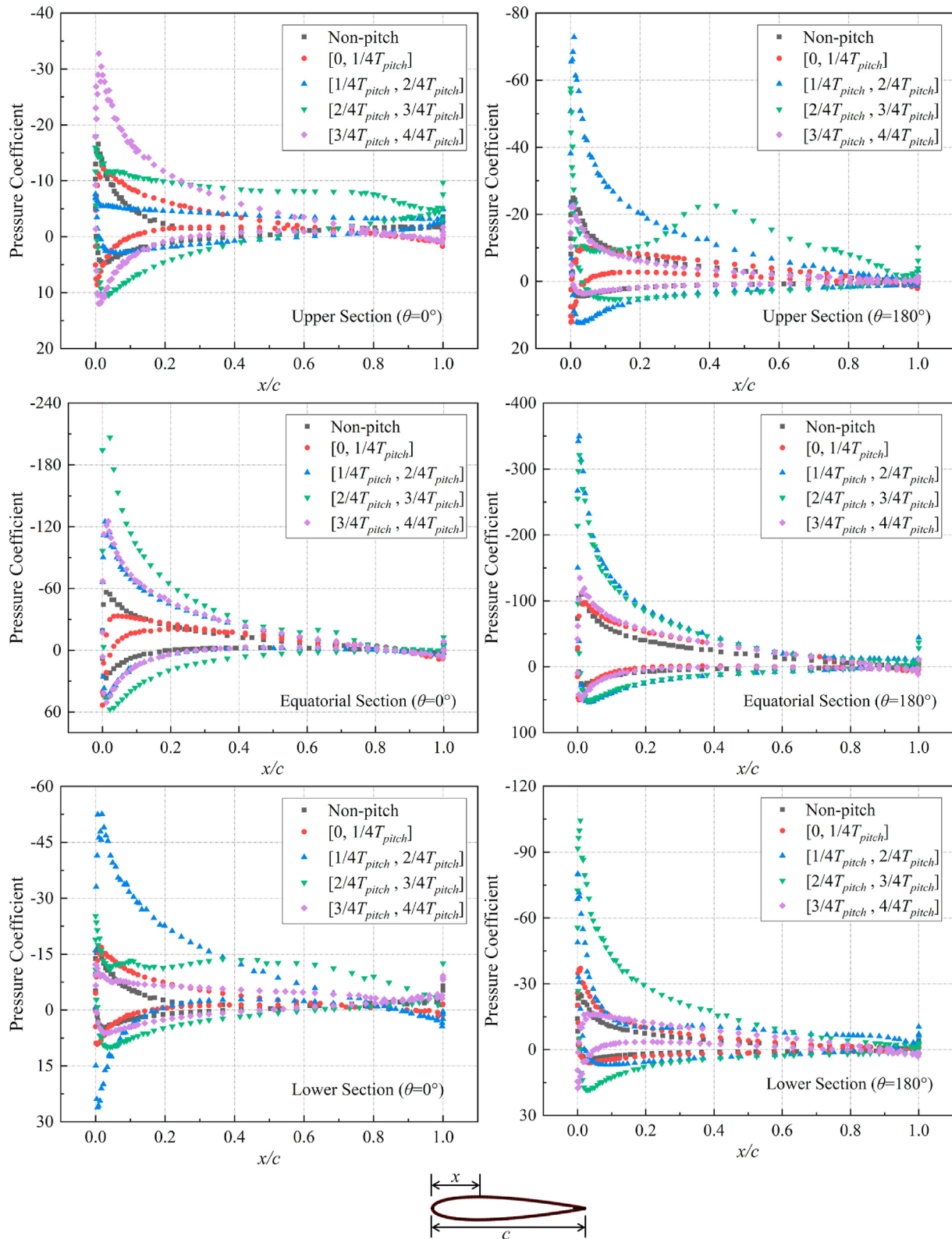


Fig. 10. The pressure coefficient distributions around the blade surface at different sections along the blade span at different azimuthal angles.

azimuthal angles in pitch motion were compared as illustrated in Fig. 10. It is noticeable that the difference in pressure coefficient distribution in the leading edge region is much more obvious than that in trailing edge region of the blade in different pitch motion

periods. Besides, it can be found that the pressure coefficient difference between the pressure side and the suction side of the lower section is significantly greater than that of the upper section at $\theta = 180^\circ$ in the period of $[1/4T_{pitch}, 2/4T_{pitch}]$ and $[2/4T_{pitch}, 3/4T_{pitch}]$. It

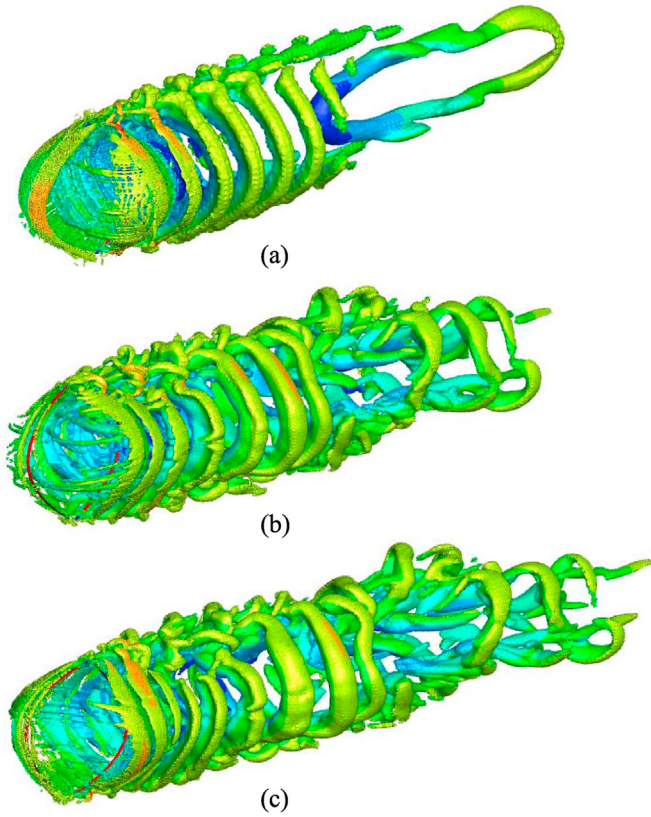


Fig. 11. Iso-Surface of turbulent vortex structure around the wind turbine for $Q = 100s^{-2}$ contoured by the velocity magnitude at $\lambda = 5.0$: (a) non-pitch; (b) pitch motion, equilibrium position; (c) pitch motion, position of pitch amplitude.

mainly attributes to the higher induced velocity at the top section of the blade, which results in the larger relative attack angle. These results are similar to the findings reported by Lei et al. [28,37]. However, the configuration of ϕ -type wind turbine makes the pressure distribution quite different at the equatorial section. The approximate parabolic outline determines that the tip speeds of the upper and lower sections of the blade are relatively small. In addition, there are also the effects of blade-tip vortex and spanwise energy dissipation, resulting in the larger pressure coefficient difference at the equatorial section. Furthermore, by comparing the pressure coefficient distributions of the same blade section at different azimuthal angles, it can be seen that the pressure coefficient difference at $\theta = 0^\circ$ is smaller than that at $\theta = 180^\circ$ in the upstream region. This is consistent with the results presented in Fig. 9.

The turbulent vortex structures around the wind turbine blade are shown in Fig. 11. It can be observed that the vortex structure of the fixed wind turbine is more stable and regular than that under pitch motion. The massive separated flow occurs over the blade span, and two strip vortices formed and shed from the blade trailing edge. For the wind turbine under pitch motion, however, numerous inclined vortex structures developed and moved downstream. Compared with the fixed wind turbine, the vortex structure around the blade tip region under pitch motion is more complicated at the equilibrium position as shown in Fig. 11(b). Due to the stronger interaction between moving blades and flow field, the vortex may break and cause a complex flow at the position of pitch angle amplitude.

Fig. 12 illustrates the vorticity distributions at the equatorial section around the two blades at different stages in one pitch motion period. It can be observed that the mild flow separation occurs on the blade surface when the blade I rotates to the position

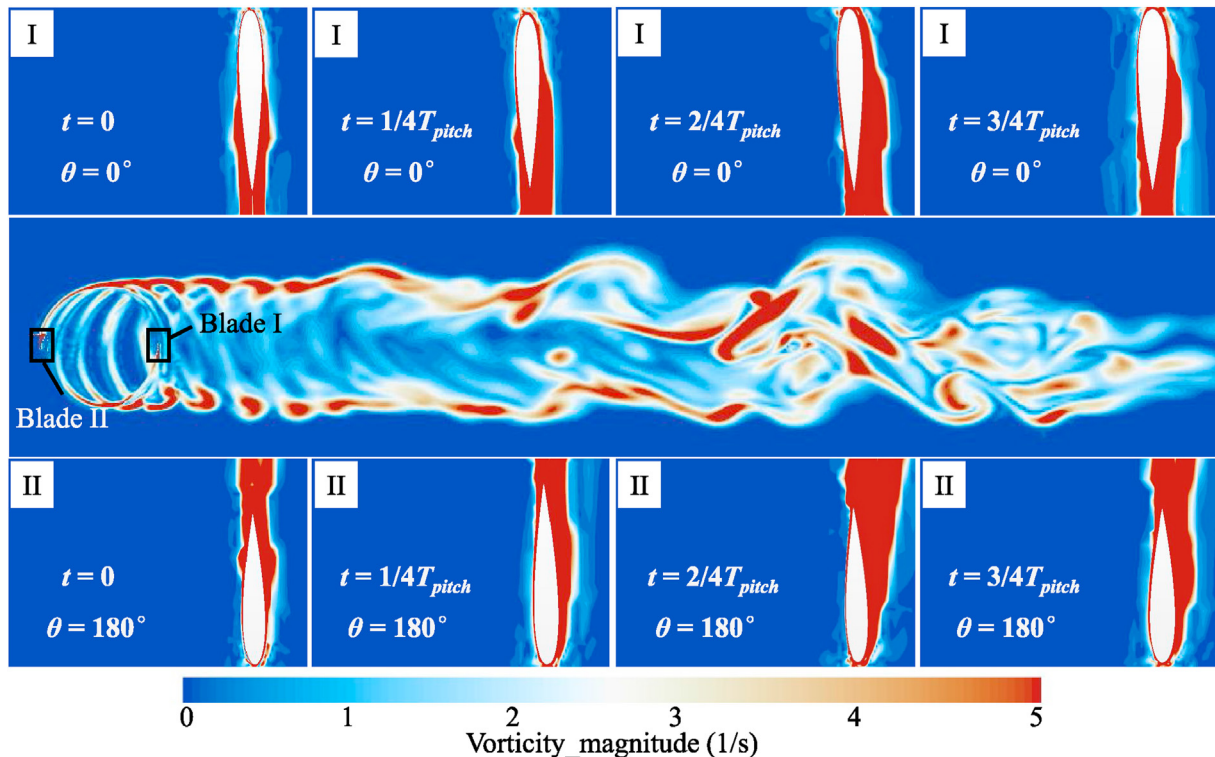


Fig. 12. The vorticity distributions at the equatorial section around the two blades at different stages in one pitch motion period.

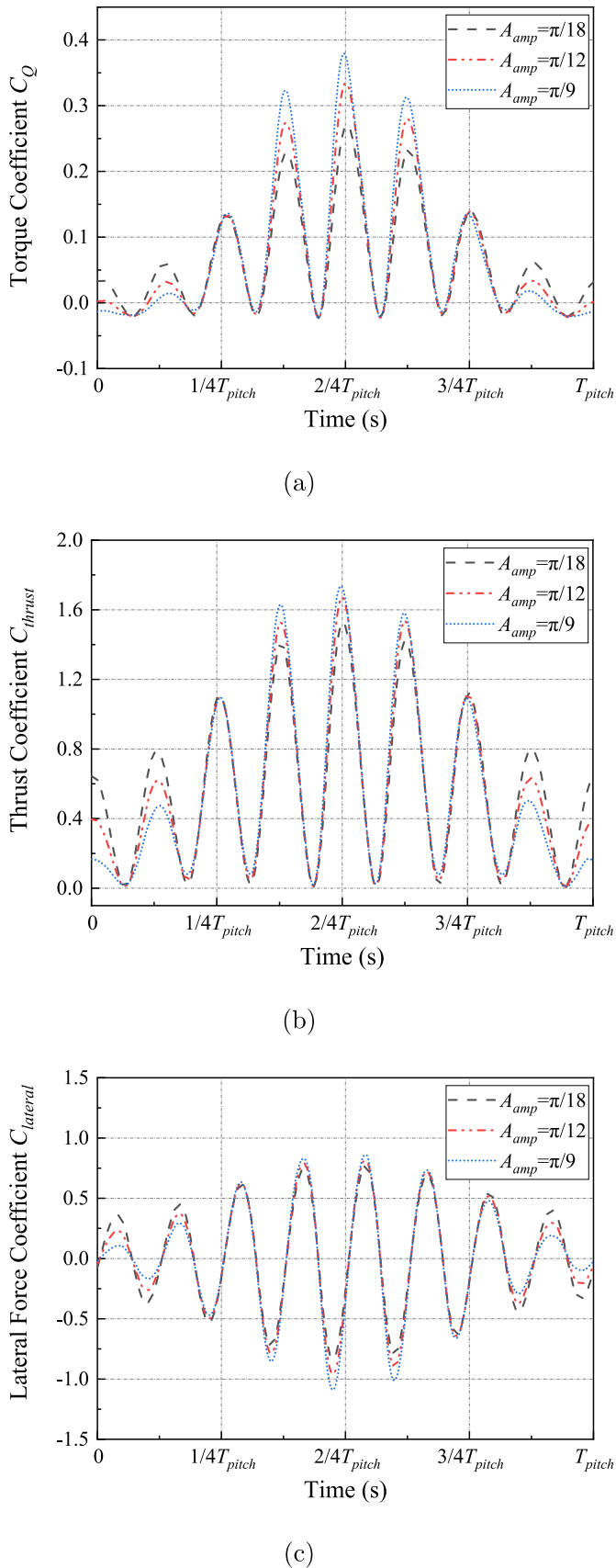


Fig. 13. The variations of force coefficients of the wind turbine under different amplitudes of pitch motion: (a) torque coefficient; (b) thrust coefficient; (c) lateral force coefficient ($\lambda = 5$, $T_{pitch} = 4T$).

Table 4

Comparison of averaged power coefficient of the wind turbine under different amplitudes of pitch motion, $\lambda = 5$, $T_{pitch} = 4T$.

Amplitude	Non-pitch	$A_{amp} = \pi/18$	$A_{amp} = \pi/12$	$A_{amp} = \pi/9$
C_p	0.3177	0.3328	0.3530	0.3746

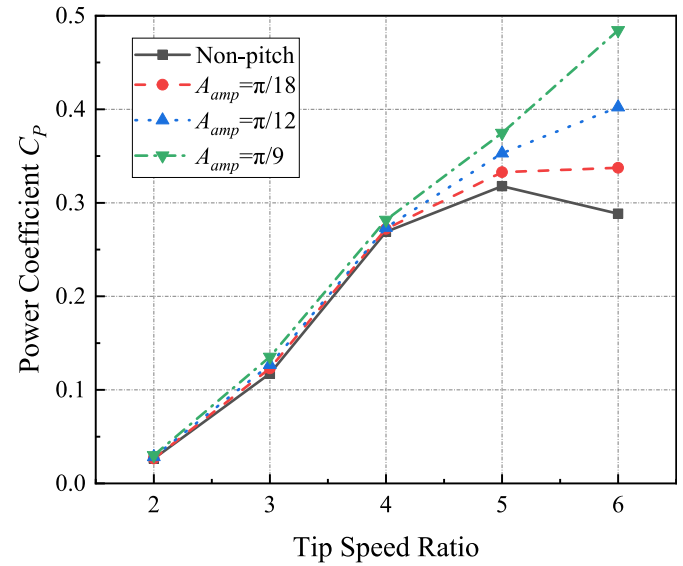


Fig. 14. The variations of angular velocity of pitch motion with different amplitudes, $T_{pitch} = 4T$.

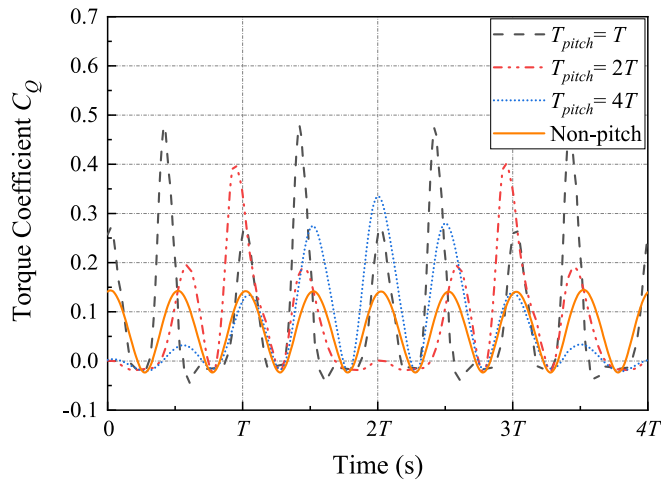
$\theta = 0^\circ$ at $t = 0$ in one pitch motion period. At $t = 1/4T_{pitch}$, stronger vortices shed from the suction side of the blade I at the same azimuthal angle of $\theta = 0^\circ$. Afterwards, the massive flow separation can be found at $t = 2/4T_{pitch}$ when the wind turbine returns to the equilibrium position. The massive flow separation is caused by the higher angle of attack resulted from the induced velocity. Similarly, the strongest vortices shedding from the surface of blade II at $\theta = 180^\circ$ occurs at $t = 2/4T_{pitch}$.

4.2. Effect of pitch motion amplitude

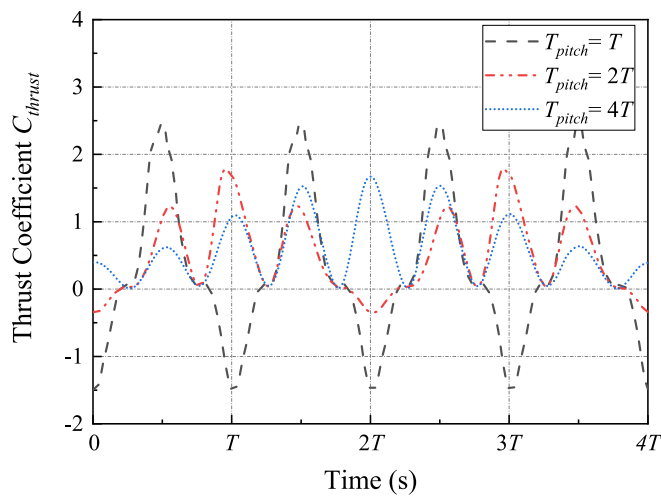
For the offshore floating wind turbine, the platform would be subjected to different wind and wave conditions. The environmental loads would be one of the main factors affecting the pitch motion characteristics of the whole VAWT, including amplitude and period. Therefore, the aerodynamic characteristics of the ϕ -type VAWT under different amplitudes and the same period of pitch motion are investigated in this subsection.

There are three different amplitudes of pitch motion tested in the study, including $A_{amp} = \pi/18$, $A_{amp} = \pi/12$, and $A_{amp} = \pi/9$. The period was set as $T_{pitch} = 4T$ and all the other parameters were kept the same in these three cases. Under these conditions, the induced velocity of the VAWT is larger at the equilibrium position as the pitch amplitude increases.

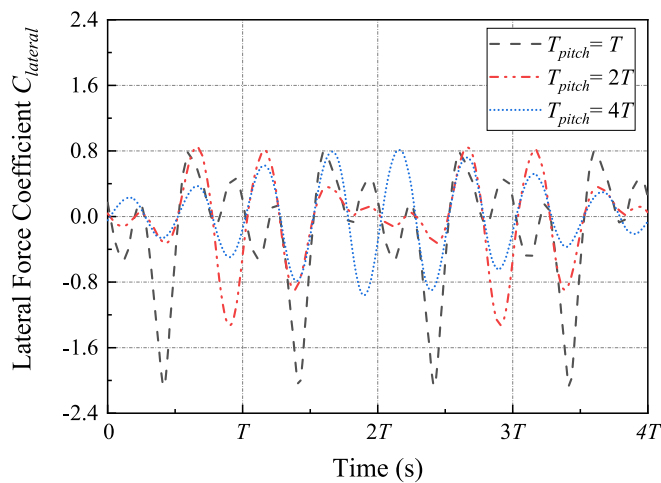
The variations of force coefficients of the wind turbine under different amplitudes of pitch motion are illustrated in Fig. 13. For the torque coefficient, the fluctuation of the coefficient curve increases with the pitch amplitude as shown in Fig. 13(a). However, the increase in torque ripple is not proportional to the increment in amplitude. The amplitude of the angular velocity for $A_{amp} = \pi/9$ is twice that of $A_{amp} = \pi/18$, while the amplitude of the torque coefficient fluctuation of $A_{amp} = \pi/9$ is about 1.5 times that of $A_{amp} =$



(a)



(b)



(c)

$\pi/18$. Besides, in the time period of $[0, 1/4T_{pitch}]$ and $[3/4T_{pitch}, 4/4T_{pitch}]$, the generated torque coefficient is lower as the pitch amplitude increases, while the torque coefficient increases with the pitch amplitude in the period of $[1/4T_{pitch}, 2/4T_{pitch}]$ and $[2/4T_{pitch}, 3/4T_{pitch}]$. The variations of thrust coefficient and the lateral force coefficient are shown in Fig. 13 (b) and (c). The trend of the thrust coefficient C_{thrust} is similar to that of torque coefficient. As for the force in the cross-wind direction, the maximum values of lateral force coefficient are almost the same for different pitch amplitudes. The main differences in $C_{lateral}$ can be found in the period of $[0, 1/4T_{pitch}]$ and $[3/4T_{pitch}, 4/4T_{pitch}]$.

To compare the power output of the studied ϕ -type VAWT under different amplitudes of pitch motion, the averaged power coefficients of the wind turbine were calculated as listed in Table 4. It can be seen that the pitch motion can increase the power coefficient of the wind turbine to a certain extent. The power coefficient increases with the pitch amplitude, and the net C_p increments corresponding to $A_{amp} = \pi/18$, $A_{amp} = \pi/12$, and $A_{amp} = \pi/9$ are 1.51%, 3.53% and 5.69%, respectively.

Besides, the effect of pitch motion amplitude was investigated at different tip speed ratios as shown in Fig. 14. It can be observed that the variation in averaged power coefficient due to wind turbine pitch motion is quiet small at low tip speed ratios. On the contrary, the platform pitch motion would effectively increase the power coefficient of wind turbine at moderate and high tip speed ratios. In addition, it is found that the influence of the pitch motion amplitude on the power output is the same under different rotation conditions.

4.3. Effect of pitch motion period

In addition to the effect of pitch amplitude, the influence of the period of pitch motion on the aerodynamic performance of the ϕ -type VAWT was evaluated. Three different periods of pitch motion ($T_{pitch} = T$, $T_{pitch} = 2T$, $T_{pitch} = 4T$, T is the rotor rotation period) were set for the wind turbine, while the pitch amplitudes were kept the same ($A_{amp} = \pi/12$). It suggests that as the pitch motion period decreases, the induced angular velocity fluctuates more intensely and the peak value increases.

Fig. 15(a) presents the variation of torque coefficient under different periods of pitch motion. The results show that as the pitch motion period decreases, the fluctuation of C_Q increases. Compared with the effect of pitch amplitude, the peaks of the three torque coefficient curves with different pitch periods have obvious phase difference. For the studied wind turbine without pitch motion, the frequency of the peak torque coefficient is about $2f$ ($f = 2\pi/T$), namely the blade pass frequency [38]. However, the fluctuation frequencies of these C_Q curves with different pitch periods are inconsistent. This phenomenon will also be discussed later. The comparisons of thrust coefficient and lateral force coefficient under different periods of pitch motion are shown in Fig. 15 (b) and (c). The results indicate that the thrust and lateral force change dramatically when the pitch motion period is equal to the rotation period ($T_{pitch} = T$). The negative value of C_{thrust} is mainly caused by the high induced velocity due to the pitch motion. As mentioned above, the induced velocity in the stationary coordinate system is much higher than the free-stream wind speed. Besides, the period of pitch motion also makes great difference in the lateral force exerting on the wind turbine. Thus, more attention should be paid

Fig. 15. The variations of force coefficients of the wind turbine under different periods of pitch motion: (a) torque coefficient; (b) thrust coefficient; (c) lateral force coefficient ($\lambda = 5$, $A_{amp} = \pi/12$).

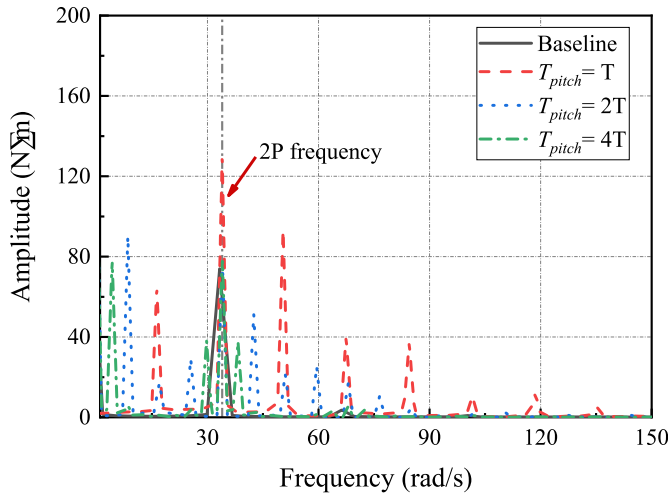


Fig. 16. Comparison of the frequency spectra of rotor torque under different periods of pitch motion ($\lambda = 5, A_{amp} = \pi/12$).

Table 5

Comparison of averaged power coefficient of the wind turbine under different periods of pitch motion, $\lambda = 5, A_{amp} = \pi/12$.

Amplitude	Non-pitch	$T_{pitch} = T$	$T_{pitch} = 2T$	$T_{pitch} = 4T$
C_p	0.3177	0.4703	0.3838	0.3530

to the fatigue load on the components of offshore VAWT.

Fig. 16 presents the generated torque of the wind turbine under different conditions in frequency domain. To obtain the characteristics in frequency domain, another 28 time-domain rotor revolutions were calculated. It is obvious that the largest amplitude of generated torque occurs at 34 rad/s, corresponding to the $n \times P$ frequency, where n is the number of blades and P is the rotational speed of wind turbine. For the studied ϕ -type two-bladed VAWT in the fixed state, there is only one peak point at 34 rad/s. However, the pitch motion of wind turbine causes many local peaks in the torque spectrum, especially the peaks occurring at integer multiples of the P frequency at $T_{pitch} = T$ (represented by the red dotted line). For other periods of pitch motion, the smaller peaks can also be found at several different frequencies, while these frequencies have not shown a certain regularity. In the preliminary design of floating wind turbine, the characteristics calculation of turbine and floating platform is usually within a quasi-static framework [39], where only the P and $n \times P$ frequencies were taken into consideration. However, the current results indicate that the coupling effect of platform motion and wind turbine rotation on aerodynamic force is a potential resonance-inducing factors.

Table 5 presents the averaged power coefficient of the ϕ -type VAWT under different periods of pitch motion to evaluate its power performance. The results show that the pitch motion would increase the power coefficient of wind turbine. The net C_p increments corresponding to $T_{pitch} = T, T_{pitch} = 2T$, and $T_{pitch} = 4T$ are 15.26%, 6.61% and 3.53%, respectively. It is noted that lesser negligible increment in turbine performance can be found with higher

Table 6

Comparison of averaged power coefficient increment of the wind turbine under different periods of pitch motion.

Parameters	Optimal tip speed ratio	$A_{amp} = \pi/12, T_{pitch} = 2T$	$A_{amp} = \pi/12, T_{pitch} = 4T$	$A_{amp} = \pi/18, T_{pitch} = 4T$
ϕ -type VAWT	2.245	20.81%	11.11%	4.57%
H-type VAWT	5.0	4.97%	3.32%	2.21%

pitching period. Similar trends for the change in power coefficient were also reported in the H-type VAWT [37] and the HAWT [40]. The increased swept area and the higher wind velocity in the downstream region could partly interpret this phenomenon [37,41]. Under the premise of ensuring the safety of the wind turbine, the increased power output can be utilized.

Finally, the increments of power coefficient of the current ϕ -type VAWT under pitch motion was compared to that of H-type VAWT reported in literature [37] as shown in Table 6. The two types of floating wind turbines are evaluated at the optimal tip speed ratio λ , where T corresponds to their respective rotation period. The results show that under the same amplitude and period of pitch motion, the increments of averaged power coefficient of the ϕ -type VAWT are higher than that of H-type VAWT. It might be due to the different structures of the two wind turbines. The movement of the straight blade caused by pitch motion would enhance the spanwise flow, resulting in greater blade tip dissipation. However, due to the curved structure of the ϕ -type wind turbine blade, the movement of the curved blade does not squeeze the air too much to the blade tip region. This may explain the higher power coefficient increment found in the ϕ -type VAWT.

5. Discussion

In the current study, the aerodynamic performance of a ϕ -type VAWT under pitch motion is investigated. The pitch motion patterns of model-scale wind turbine given in this study could be converted by utilizing the Froude scaling, which is typically used in the scaling of offshore structures [16]. On the other hand, the Reynolds similitude is usually achieved by using the same lift and drag coefficients of blade or ensuring that the measured Reynolds number is basically at the same magnitude [42, 43]. While the computational models reported for offshore HAWT in recent years are large-scale wind turbines [44,45], the results from the up-scaled model should be the same as that of the small-scale wind turbine if the scaling laws are consistent [43]. But it should also be acknowledged that the ratio of the pitching period to the revolution period of a small-scale wind turbine is not exactly the same as that of the large-scale wind turbine. The operating characteristics of wind turbine set in this study are just one of the practical engineering cases. However, the changes in the aerodynamic characteristics found in this study might be still significant in actual engineering conditions, although the Reynolds number would not be fully consistent when the Froude scaling was applied.

The effect of pitch motion on the ϕ -type VAWT is noticeable for both instantaneous force coefficients and averaged loads on the rotor. It is found that the force-time history curve changes periodically during the pitch motion of the wind turbine. The amplitude of the torque coefficient ripples shows periodic characteristics. The averaged power output of the VAWT under pitch motion is larger than that of the fixed wind turbine, and the net power coefficient increment is about 1.5%–15%. The similar conclusions were reported in other studies on offshore wind turbines [37,46]. This means that the offshore floating wind turbine could extract and convert more wind energy into electricity without considering the structural dynamic response.

In the six-degree-of-freedom of offshore VAWT, it is generally

considered that the pitch motion, surge motion and yaw motion are typical motion patterns. From the existing literature, it can be found that the effects of surge motion and pitch motion on wind turbine aerodynamics had similar laws [28,37,47]. Besides, the equivalent wind shear induced by pitch motion was found to make severer fluctuations to the apparent wind speed and aerodynamic loads on the rotor [40]. However, the relationship behind these phenomena has not been clearly demonstrated. In fact, the effect of pitch motion on the aerodynamics of wind turbine can be regarded as the combined effect of surge motion and heave motion. In the pitch motion, the tangential linear velocity of the blade relative to the axis of pitch motion can be decomposed into the velocity in surge direction and heave direction. When the amplitude of pitch motion is small ($< \pi/12$), the velocity in heave direction is much lower than that in surge direction. Therefore, the effect of pitch motion on aerodynamic forces was found to be similar to that of surge motion. In addition, although the instantaneous angular velocity of the entire rotor caused by the pitch motion is the same, the relative velocity along the height of the blade is different due to the induced vertical wind shear effect. It increases the fluctuation of aerodynamic forces on the blade which might introduce fatigue damages to the wind turbine components [40].

The pitch motion of VAWT is found to increase the fluctuation amplitude of the generated torque. How to maintain the stable output and suppress the fatigue loads on floating wind turbine has always been a key issue. For this problem, researchers have done a lot of work for the HAWTs, and many mature control technologies have also appeared [48]. However, due to the complicated aerodynamic characteristics of VAWTs, many technologies that have been successfully applied to HAWTs are still in the experimental stage on VAWTs. Only a few control schemes were proposed and have not been applied to practical engineering [49]. This means that more attention should be paid to the servo control system of floating VAWT in future research.

Furthermore, the effect of pitch period on the aerodynamic forces of wind turbine is found to be more significant than that of pitch amplitude. Compared with the value of aerodynamic forces, more attention should be paid to the changes in the peak frequency due to the pitch motion. This is because it involves the vibration and resonance issues to be considered in the design process [50]. As we known, it is important to separate the natural frequencies of the wind turbine from the excitation frequencies to avoid resonance and reduce vibration. The $n \times P$ frequency of the VAWT is relatively closer to the wave spectra peak frequencies, while the $n \times P$ frequency of the HAWT is usually much higher than the typical wave spectra peak frequencies [47]. This brings more difficulties to the design of offshore VAWT. In the previous studies [22,51], research was more focused on the power spectra of six degrees of freedom motion of floating wind turbine. However, the current study shows that the frequency of the peak torque coefficient would change under different periods of pitch motion which has been rarely noticed. It means that more limitations should be imposed on the designed natural frequency range of the offshore wind turbine. In addition to the structural design of the main components of wind turbine, for both offshore VAWT and HAWT, the correlation between the unsteady aerodynamic phenomena and the non-stationary dynamics vibration should also be considered in the generator system, including in the mechanical gearing system [52].

6. Conclusions

The effect of pitch motion on the aerodynamic performance of ϕ -type VAWT was investigated in this study by using the validated IDDES SST $k-\omega$ turbulence model. A series of pitch motion

patterns were analyzed, and the effect of the amplitude and period of pitch motion was discussed. The main conclusions can be drawn as follows.

- The pitch motion of VAWT increases the power output of the wind turbine. The averaged net power coefficient increment is about 1.5%–15%. The fluctuation of the peak torque coefficient is mainly caused by the variation of the relative local velocity.
- The effect of pitch motion on the aerodynamics of wind turbine can be regarded as the combined effect of surge motion and heave motion, in which the surge-like motion plays a major role. It explains the similarity of the effects of pitch motion and surge motion on wind turbine aerodynamics.
- While increasing the averaged power output of VAWT, the pitch motion greatly increases the aerodynamic fluctuations, including torque, thrust and lateral force, which is not conducive to structural safety. This needs to be improved with more advanced controllers to maintain a stable output in the future study.
- The effect of pitch period on wind turbine aerodynamics is more significant than that of pitch amplitude. It is found that the value and frequency of peak force of VAWT change under pitch motion. The change in frequency would put greater restrictions on the designed natural frequency of floating wind turbine to avoid resonance and reduce vibration.

Overall, the results of the current study provide additional information about the effect of pitch motion on wind turbine aerodynamics. As also recommended above, future research on the effect of the unsteady aerodynamics caused by wind turbine motion on structural response is warranted.

Credit author statement

Jie Su: Conceptualization, Writing – original draft, Writing-Reviewing and Editing. Yu Li: Data curation, Software. Yaoran Chen: Formal analysis, Software. Zhaolong Han: Writing- Reviewing and Editing, Project administration. Dai Zhou: Supervision, Project administration. Yan Bao: Methodology. Yongsheng Zhao: Validation.

Declaration of competing interest

The authors declare that they have no known competing financial interests or personal relationships that could have appeared to influence the work reported in this paper.

Acknowledgments

The financial supports from the Innovation Program of Shanghai Municipal Education Commission(No. 2019-01-07-00-02-E00066), National Natural Science Foundation of China (Nos. 42076210, 51879160, 11772193 and 51809170), Program for Professor of Special Appointment (Eastern Scholar) at Shanghai Institutions of Higher Learning, the Oceanic Interdisciplinary Program of Shanghai Jiao Tong University (No. SL2020PT201), Shuguang Program supported by Shanghai Education Development Foundation and Shanghai Municipal Education Commission (No.19SG10), and Shanghai Natural Science Foundation (No. 18ZR1418000) are gratefully acknowledged.

References

- [1] Kaldellis JK, Zafirakis D. The wind energy (r) evolution: a short review of a long history. *Renew Energy* 2011;36:1887–901.

- [2] Pérez-Collazo C, Greaves D, Iglesias G. A review of combined wave and offshore wind energy. *Renew Sustain Energy Rev* 2015;42:141–53.
- [3] Kaldellis J, Apostolou D, Kapsali M, Kondili E. Environmental and social footprint of offshore wind energy. comparison with onshore counterpart. *Renew Energy* 2016;92:543–56.
- [4] Ghasemian M, Ashrafi ZN, Sedaghat A. A review on computational fluid dynamic simulation techniques for darrieus vertical axis wind turbines. *Energy Convers Manag* 2017;149:87–100.
- [5] Kumar R, Raahemifar K, Fung AS. A critical review of vertical axis wind turbines for urban applications. *Renew Sustain Energy Rev* 2018;89:281–91.
- [6] Yang H, Zhu Y, Lu Q, Zhang J. Dynamic reliability based design optimization of the tripod sub-structure of offshore wind turbines. *Renew Energy* 2015;78:16–25.
- [7] Wang X, Zeng X, Yang X, Li J. Feasibility study of offshore wind turbines with hybrid monopile foundation based on centrifuge modeling. *Appl Energy* 2018;209:127–39.
- [8] Borg M, Collu M. Offshore floating vertical axis wind turbines, dynamics modelling state of the art. part iii: hydrodynamics and coupled modelling approaches. *Renew Sustain Energy Rev* 2015;46:296–310.
- [9] Martin HR, Kimball RW, Viselli AM, Goupee AJ. Methodology for wind/wave basin testing of floating offshore wind turbines. *J Offshore Mech Arctic Eng* 136.
- [10] Sebastian T, Lackner M. Analysis of the induction and wake evolution of an offshore floating wind turbine. *Energies* 2012;5:968–1000.
- [11] Hu Zq, Liu Y, Wang J. An integrated structural strength analysis method for spar type floating wind turbine. *China Ocean Eng* 2016;30:217–30.
- [12] Li L, Cheng Z, Yuan Z, Gao Y. Short-term extreme response and fatigue damage of an integrated offshore renewable energy system. *Renew Energy* 2018;126:617–29.
- [13] Karikomi K, Ohta M, Nakamura A, Iwasaki S, Hayashi Y, Honda A. Wind tunnel testing on negative-damped responses of a 7mw floating offshore wind turbine. Poster presented at EWEA Offshore .
- [14] Goupee AJ, Kimball RW, Dagher HJ. Experimental observations of active blade pitch and generator control influence on floating wind turbine response. *Renew Energy* 2017;104:9–19.
- [15] Azcona J, Bouchotrouch F, González M, Garcíandía J, Munduate X, Kelberlau F, et al., Aerodynamic thrust modelling in wave tank tests of offshore floating wind turbines using a ducted fan. *J Phys Conf*, vol. 524, 012089.
- [16] Coulling AJ, Goupee AJ, Robertson AN, Jonkman JM, Dagher HJ. Validation of a fast semi-submersible floating wind turbine numerical model with deepwind test data. *J Renew Sustain Energy* 2013;5:023116.
- [17] Viselli AM, Goupee AJ, Dagher HJ, Allen CK. Design and model confirmation of the intermediate scale volturnus floating wind turbine subjected to its extreme design conditions offshore Maine. *Wind Energy* 2016;19:1161–77.
- [18] Koo BJ, Goupee AJ, Kimball RW, Lambrakos KF. Model tests for a floating wind turbine on three different floaters. *J Offshore Mech Arctic Eng* 136.
- [19] Madsen F, Nielsen T, Kim T, Bredmose H, Pegalajar-Jurado A, Mikkelsen R, et al., Experimental analysis of the scaled dtu10mw tlp floating wind turbine with different control strategies. *Renewable Energy* .
- [20] Paquette JA, Barone MF. Innovative offshore vertical-axis wind turbine rotor project. Tech. rep. Albuquerque, NM (United States): Sandia National Lab.(SNL-NM); 2012.
- [21] Borg M, Collu M. A comparison on the dynamics of a floating vertical axis wind turbine on three different floating support structures. *Energy Procedia* 2014;53:268–79.
- [22] Wang K, Moan T, Hansen MO. Stochastic dynamic response analysis of a floating vertical-axis wind turbine with a semi-submersible floater. *Wind Energy* 2016;19:1853–70.
- [23] Cheng Z, Madsen HA, Gao Z, Moan T. Effect of the number of blades on the dynamics of floating straight-bladed vertical axis wind turbines. *Renew Energy* 2017;101:1285–98.
- [24] Guo Y, Liu Lq, Li Y, Xiao Cs, Tang Yg. The surge-heave-pitch coupling motions of the ϕ -type vertical axis wind turbine supported by the truss spar floating foundation. *J Hydrodyn* 2019;31:669–81.
- [25] Jonkman JM. Dynamics of offshore floating wind turbines: a model development and verification. *Wind Energy: An International Journal for Progress and Applications in Wind Power Conversion Technology* 2009;12:459–92.
- [26] Hand B, Cashman A, Kelly G. A low-order model for offshore floating vertical axis wind turbine aerodynamics. *IEEE Trans Ind Appl* 2016;53:512–20.
- [27] Lei H, Zhou D, Bao Y, Li Y, Han Z. Three-dimensional improved delayed detached eddy simulation of a two-bladed vertical axis wind turbine. *Energy Convers Manag* 2017;133:235–48.
- [28] Lei H, Zhou D, Bao Y, Chen C, Ma N, Han Z. Numerical simulations of the unsteady aerodynamics of a floating vertical axis wind turbine in surge motion. *Energy* 2017;127:1–17.
- [29] Bedon G, Paulsen US, Madsen HA, Belloni F, Castelli MR, Benini E. Computational assessment of the deepwind aerodynamic performance with different blade and airfoil configurations. *Appl Energy* 2017;185:1100–8.
- [30] Sheldahl RE, Klimas PC, Feltz LV. Aerodynamic performance of a 5-metre-diameter Darrieus turbine with extruded aluminum NACA-0015 blades. National Technical Information Service USA; 1980.
- [31] Paraschivoiu I. Wind turbine design: with emphasis on Darrieus concept. Presses inter Polytechnique; 2002.
- [32] Thé J, Yu H. A critical review on the simulations of wind turbine aerodynamics focusing on hybrid rans-les methods. *Energy* 2017;138:257–89.
- [33] Su J, Chen Y, Han Z, Zhou D, Bao Y, Zhao Y. Investigation of v-shaped blade for the performance improvement of vertical axis wind turbines. *Appl Energy* 2020;260:114326.
- [34] Su J, Lei H, Zhou D, Han Z, Bao Y, Zhu H, et al. Aerodynamic noise assessment for a vertical axis wind turbine using improved delayed detached eddy simulation. *Renew Energy* 2019;141:559–69.
- [35] Chen Y, Su J, Han Z, Zhao Y, Zhou D, Yang H, et al. A shape optimization of ϕ -shape darrieus wind turbine under a given range of inlet wind speed. *Renew Energy* 2020;159:286–99.
- [36] Collu M, Borg M, Shires A, Rizzo FN, Lupi E, Flovawt: Further progresses on the development of a coupled model of dynamics for floating offshore vawts. International Conference on Offshore Mechanics and Arctic Engineering, American Society of Mechanical Engineers, vol. 45547, V09BT09A044.
- [37] Lei H, Zhou D, Lu J, Chen C, Han Z, Bao Y. The impact of pitch motion of a platform on the aerodynamic performance of a floating vertical axis wind turbine. *Energy* 2017;119:369–83.
- [38] Negm HM, Maalawi KY. Structural design optimization of wind turbine towers. *Comput Struct* 2000;74:649–66.
- [39] Vita L. Offshore vertical axis wind turbine with floating and rotating foundation .
- [40] Wen B, Dong X, Tian X, Peng Z, Zhang W, Wei K. The power performance of an offshore floating wind turbine in platform pitching motion. *Energy* 2018;154:508–21.
- [41] Chowdhury AM, Akimoto H, Hara Y. Comparative cfd analysis of vertical axis wind turbine in upright and tilted configuration. *Renew Energy* 2016;85:327–37.
- [42] Martin HR. Development of a scale model wind turbine for testing of offshore floating wind turbine systems.
- [43] Jain A, Goupee AJ, Robertson AN, Kimball RW, Jonkman JM, Swift AH, et al., Fast code verification of scaling laws for deepwind floating wind system. The Twenty-second international offshore and Polar engineering Conference, International Society of Offshore and Polar Engineers.
- [44] Tran TT, Kim DH. Fully coupled aero-hydrodynamic analysis of a semi-submersible fowt using a dynamic fluid body interaction approach. *Renew Energy* 2016;92:244–61.
- [45] Salehyar S, Li Y, Zhu Q. Fully-coupled time-domain simulations of the response of a floating wind turbine to non-periodic disturbances. *Renew Energy* 2017;111:214–26.
- [46] Leble V, Barakos G. 10-mw wind turbine performance under pitching and yawing motion. *J Sol Energy Eng* 139.
- [47] Borg M, Collu M. Frequency-domain characteristics of aerodynamic loads of offshore floating vertical axis wind turbines. *Appl Energy* 2015;155:629–36.
- [48] Zhang M, Li X, Tong J, Xu J. Load control of floating wind turbine on a tension-leg-platform subject to extreme wind condition. *Renew Energy* 2020;151:993–1007.
- [49] Merz K, Svendsen H. A control algorithm for the deepwind floating vertical-axis wind turbine. *J Renew Sustain Energy* 2013;5:063136.
- [50] McLaren K, Tullis S, Ziada S. Measurement of high solidity vertical axis wind turbine aerodynamic loads under high vibration response conditions. *J Fluid Struct* 2012;32:12–26.
- [51] Cheng Z, Madsen HA, Chai W, Gao Z, Moan T. A comparison of extreme structural responses and fatigue damage of semi-submersible type floating horizontal and vertical axis wind turbines. *Renew Energy* 2017;108:207–19.
- [52] Mabrouk IB, El Hami A, Walha L, Zghal B, Haddar M. Dynamic vibrations in wind energy systems: application to vertical axis wind turbine. *Mech Syst Signal Process* 2017;85:396–414.